Materials Chemistry and Physics 325 (2024) 129765

Contents lists available at ScienceDirect

Materials Chemistry and Physics

journal homepage: www.elsevier.com/locate/matchemphys

Influence of the as quenched state and tempering temperature on the final microstructure and hardness of a high strength medium carbon steel

Ehsan Tolouei [a], Valentin Hurel [b], Abdelhalim Loucif [a], Jean-Benoit Morin [b], Mohammad Jahazi [a,*]

[a] Department of Mechanical Engineering, École de Technologie Supérieure ÉTS, 1100 Notre-Dame St. W, Montreal, QC, H3C 1K3, Canada
[b] Finkl Steel-Sorel, 100 McCarthy, Saint-Joseph-de-Sorel, QC, J3R 3M8, Canada

HIGHLIGHTS

- Martensite reacts differently to non-isothermal tempering than bainite.
- Formation of aggregated carbide zones correlate to incomplete bainitic phase transformation and retained austenite.
- Fresh martensite formation during the final cooling of bainite tempering increases hardness compared to as-quenched bainite.

GRAPHICAL ABSTRACT

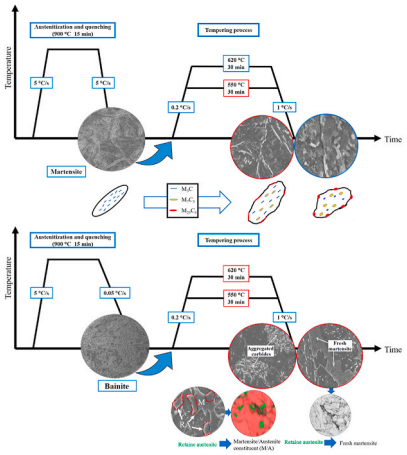

ARTICLE INFO

Keywords:
Retained austenite
Bainite
Fresh martensite
Carbides
Martensite/ austenite constituent (M/A)

ABSTRACT

The present study aimed to investigate the impact of the as-quenched microstructure and tempering temperature on the final microstructure and hardness of a medium-carbon, low-alloy steel using dilatometry, Electron backscatter diffraction (EBSD) and scanning electron microscopy (SEM). The results revealed substantial differences in the continuous heating stage of tempering in bainitic and martensitic samples, primarily attributed to the auto-tempering process during cooling. Tempering was carried out at 550 and 620 °C, and dilatometry results, along with microstructure analysis, indicated incomplete decomposition of retained austenite (RA) at both temperatures during a 30-min hold in the bainitic sample. The results show that non-decomposed RA, following the tempering of bainite, transformed into blocky fresh martensite, while no evidence of fresh martensite was observed in the martensitic sample. A new approach using EBSD and SEM images revealed that the decomposition of M/A (martensite/austenite constituent) zones in the bainitic sample resulted in the formation of a chain of aggregated chromium carbide zones at the grain boundaries. In contrast, the martensitic zone exhibited a

* Corresponding author.
E-mail address: mohammad.jahazi@etsmtl.ca (M. Jahazi).

https://doi.org/10.1016/j.matchemphys.2024.129765
Received 22 May 2024; Received in revised form 21 July 2024; Accepted 24 July 2024
Available online 28 July 2024

uniform distribution of carbides in the microstructure. The stability of the phases was examined using the TCFE10 (thermodynamics) and MOBFE5 (mobility) modules of the DICTRA Themo-Calc software. Hardness measurements on all samples indicated decreases by about 18–24 % in the martensitic sample after tempering, while the bainitic sample exhibited a 5 % increase in hardness after tempering, attributed to secondary hardening and fresh martensite formation.

1. Introduction

Bumpers and dashboards used in the automotive and truck manufacturing industries, are produced through plastic injection molding. The dies used for such operations are made of medium-carbon steels. In recent years the demand for larger parts has significantly increased and therefore, the die steels, made in the form of parallelepipedal blocks, need to be much larger than before. Moreover, the requirements for the final properties have seen an evolution in recent years. For example, superior Charpy impact and fatigue lives are required by the transportation industry.

These large blocks are manufactured through ingot casting, open-die forging, and quenching followed by tempering process [1–4]. A significant challenge encountered in the production of such blocks is related to their thicknesses. Indeed, the high thickness of these components results in the formation of temperature gradients during the quenching process, causing variations in the nature of formed phases between the surface and the core of the block [5,6]. The differences in the as-quenched microstructure coupled with subsequent tempering, pose challenges throughout the manufacturing process to achieve uniform mechanical properties, particularly in terms of hardness [5,7].

In the manufacturing process, tempering stands as the final stage, playing a significant role in determining the ultimate microstructure and mechanical properties of the material. The primary aim of the tempering process is to reduce or eliminate undesired phases such as retained austenite (RA), enhance the material's ductility, and moderate the hardness based on the intended application [8]. This is achieved by reducing the carbon (C) supersaturation in the martensitic and bainitic constituents through carbon segregation, decomposition of the RA, precipitation of carbides, and finally coarsening and spheroidization of carbides [3]. On the other hand, there are numerous issues in the tempering process: 1) formation of fresh martensite or bainite during the final cooling to room temperature after tempering [9,10]; 2) coalescence of small carbides into large size ones [9,11,12]; and 3) incomplete decomposition of RA [12]. As a result, selecting the proper tempering temperature and time is crucial for obtaining uniform microstructures and mechanical properties.

It is worth noting, the kinetics of tempering are significantly affected by the carbon concentration in the different components of the microstructure. Since the very early stages of tempering, carbon diffuses into microstructural defects such as grain boundaries, and various types of carbides (M_3C, M_2C, M_7C_3, and $M_{23}C_6$) are formed [13–17]. This process can occur during the continuous heating stage, isothermal tempering, and auto-tempering during continuous cooling. Therefore, as part of the tempering process, precipitation plays an important role in affecting the microstructure. For instance, Barrow et al. [18], reported a correlation between tempering time and the size, as well as the aspect ratio of carbides, and how these factors contribute to the ultimate mechanical properties of the material. Mayer et al. [19] examined the influence of the as-quenched microstructure range from full martensite to full bainite in medium-carbon, medium-alloy steel. Their findings revealed that the formation of M_7C_3 carbides at the lath boundaries increases when transitioning from a fully martensitic sample to a fully bainite one. Talebi et al. [3] observed needle-like carbides in as-quenched microstructure of a large size forged slab and related it to auto-tempering within the bainitic microstructure. These carbides were found to be rich in iron (Fe) with almost no presence of chromium (Cr) [3], indicating that they are most probably cementite particles. Ning et al. also noted precipitation as a result of auto-tempering in the coarse lath martensitic microstructure of a low-carbon, low-alloy steel, identifying it as transition carbides and cementite [20]. Upon reaching the target tempering temperature at the end of the continuous heating, precipitation, decomposition of RA, and coarsening continued. However, the mechanism can be influenced by the as-quenched microstructure. For instance, in a martensitic microstructure, decomposition of RA and precipitation along grain boundaries, are the dominant mechanisms [21]. Conversely, in a bainitic microstructure, alongside the decomposition of RA, the martensite-austenite constituent (M/A) assumes the principal role in the tempering process of bainite [22]. As a consequence, choosing a tempering temperature that is appropriate for the bainitic microstructure is crucial to ensuring that M/A islands are completely decomposed. Failure to temper adequately could result in elevated stress concentrations at the M/A interface, heightening the risk of crack formation during Charpy impact testing [22]. Furthermore, the formation of new martensite following tempering leads to non-uniformity in both microstructure and mechanical properties [23].

Therefore, it is of great importance to investigate the influence of tempering temperature on the type, morphology, size, and distribution characteristics of carbide precipitation in both bainitic and martensitic microstructures, especially in the context of large-size components. Notably, the investigations on as-quench microstructure and tempering temperature effects have largely focused on different grades of steel, leaving the impact of the above-mentioned parameters unexplored within the same grade of steel. Furthermore, the majority of prior studies have concentrated on precipitation after isothermal tempering, where the formation of auto-tempered carbides during cooling, and continuous heating tempering process should be considered, and very little or no data has been published on the evolution of the microstructure during the continuous heating stage of the tempering process. This stage is of high importance when it comes to large size blocks, as the continuous, or non-isothermal, heating stage is very long and could be the longest step of the tempering cycle.

The present paper addresses the above gaps in the literature and aims to determine the influence of the as-quenched microstructures and tempering temperature on the final microstructure of large size blocks. The initial section will explore the phenomena during continuous heating stages by dilatometry. Subsequently, the second part will involve a comparison between the as-quenched and tempered microstructures. Finally, the investigation will extend to the impact of tempering on hardness.

2. Materials and methods

The chemical composition of the studied steel is provided in Table 1. The original material was an as-forged slab, provided by Finkl Steel-Sorel, Quebec (Canada). Cylindrical samples of 10 mm length and 4 mm diameter were machined for dilatometry tests. All the heat treatment cycles were performed using a high-resolution TA DIL 805A/D dilatometer (TA instruments, New Castle, DE, USA). Prior to the tempering experiments, the specimens were austenitized by heating

Table 1
Chemical composition of the studied steel (wt. %).

C	Mn	Si	Ni	Cr	Mo	Micro-alloys	Fe
0.26	1.15	0.35	0.70	1.50	0.55	<0.2	Balance

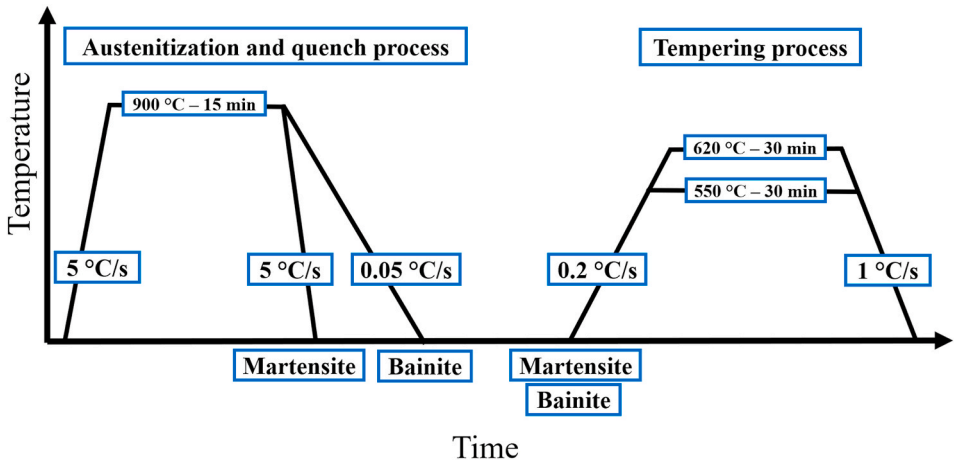

Fig. 1. Schematic of the heat treatment parameters applied in this study.

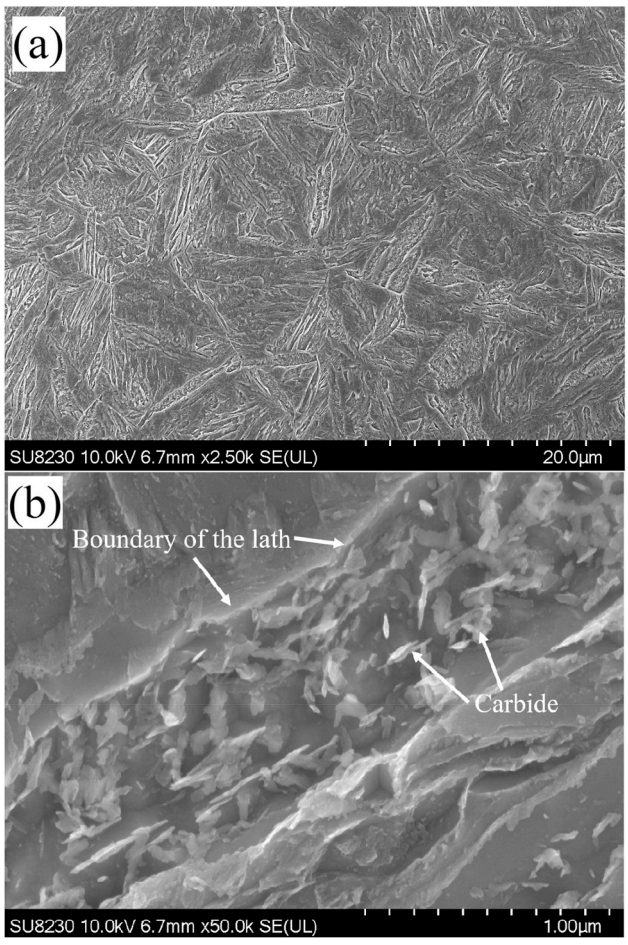

Fig. 2. SEM observation of martensitic microstructure before tempering, obtained after austenitization at 900 °C and cooling at the rate of 5 °C/s at lower magnification (a), and carbides distribution within the martensitic lath at higher magnification (b).

them up to 900 °C with a rate of 5 °C/s, held for 15 min for homogenization and then cooled to room temperature with cooling rates of 5 and 0.05 °C/s which produced a microstructure of martensite and bainite, respectively. Immediately after cooling, samples were heated with a heating rate of 0.2 °C/s up to isothermal tempering temperatures of 550 °C or 620 °C with 30 min holding times. Finally, they were cooled

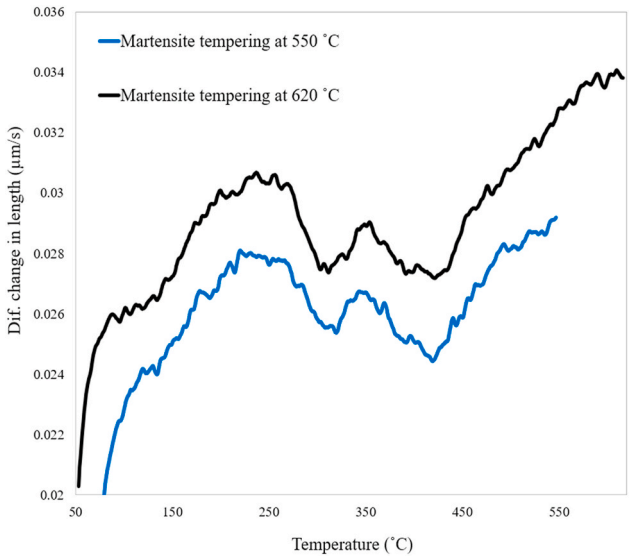

Fig. 3. Differential change in length versus temperature during continuous heating of martensite for tempering at 550 and 620 °C.

to room temperature at a rate of 1 °C/s. In laboratory experiments, small samples had the same as-quenched microstructure as large industrial blocks, and the tempering temperatures were identical for both the small samples and large blocks. Fig. 1 shows the schematic of the heat treatment cycle that was applied. It should be noted that the examination of the impact of tempering on the microstructure involved an investigation of the as-quenched microstructures as well. The dilatometry tests were performed under vacuum to avoid any oxidation and decarburization.

The samples were then prepared through conventional polishing procedures and etched with Nital 5 % solution. Electron backscatter diffraction (EBSD) and scanning electron microscopy (SEM) were carried out for the microstructure analysis, using a Hitachi-SU8230 Field Emission Gun SEM (FEG-SEM) (Hitachi, Tokyo, Japan) equipped with an energy dispersion spectrometer (EDS). Sample preparation for the EBSD analysis was done using ion beam milling (IM 4000Plus, Hitachi). In this study, to obtain a detailed microstructure analysis, SEM and EBSD were carried out simultaneously at the same location. This procedure includes conducting macro hardness tests on the sample in the form of a grid pattern. Subsequently, EBSD is performed in a specific region between the indented hardness points. The distance from the EBSD examined region to the indentations is measured in order to exactly identify the examined region of the microstructure. Utilizing this

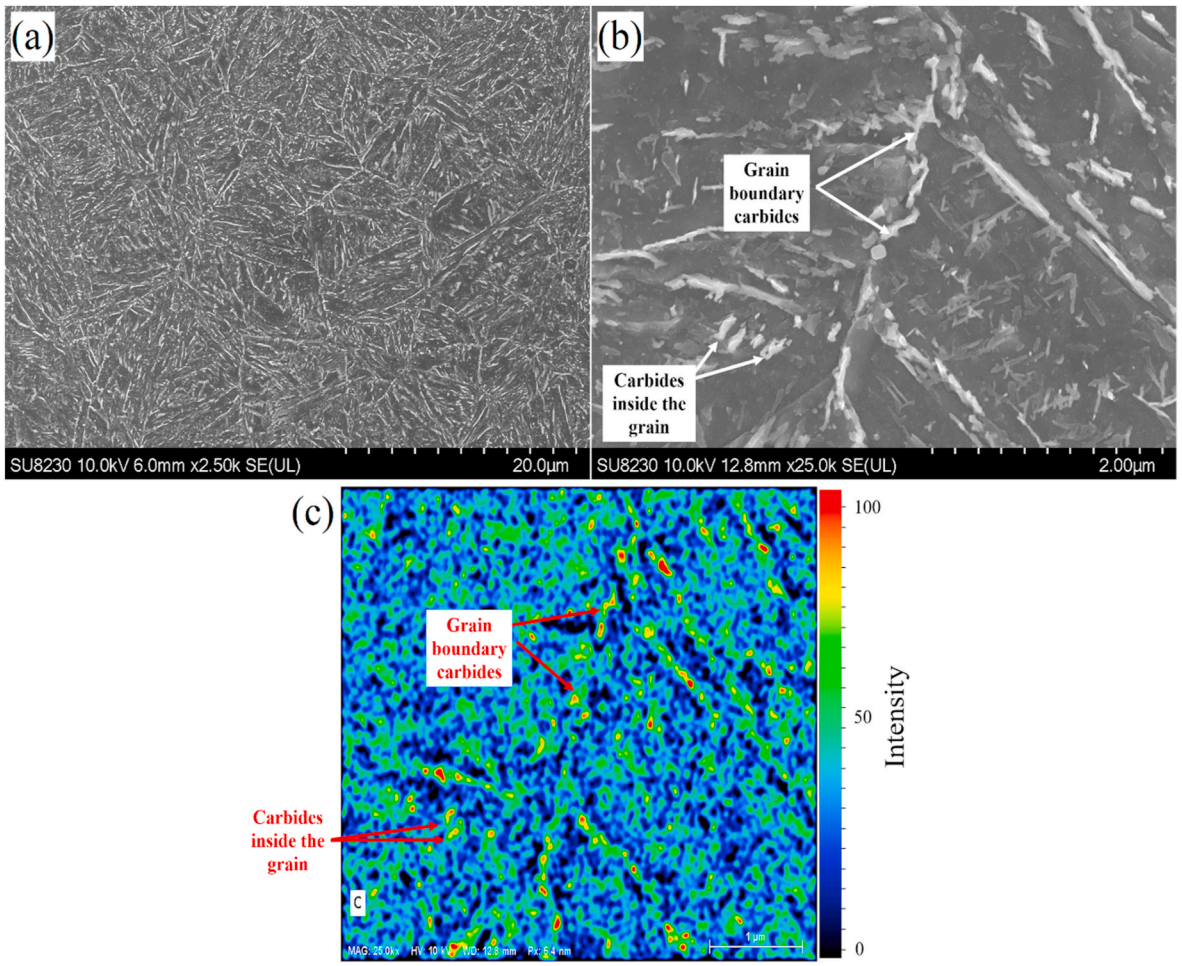

Fig. 4. SEM observation of martensitic microstructure after tempering at 550 °C in lower magnification (a), grain boundaries in higher magnification (b), and EDS mode based on carbon distribution of image b (c).

procedure, once the EBSD map was obtained, the sample was etched with a 5 % Nital solution and SEM analysis was carried out on the EBSDed areas based on the measured locations.

The Average Vickers hardness of each sample was measured on the polished surface from 10 measurements using a load of 300 g and 15 s dwell time. In order to investigate the thermodynamic stability of phases, DICTRA module of the Thermo-Calc software based on TCFE10 (thermodynamics) and MOBFE5 (mobility) database was used [24].

3. Results and discussion

3.1. Tempering of martensite

3.1.1. Initial microstructure of martensite

Fig. 2 shows as-quenched martensite microstructure, which contains auto-tempered microstructure [25]; lath-like martensite composed of carbides and the primary austenite grain boundaries. The laths are composed of lamellar precipitates oriented in two directions (Fig. 2 (b)): one along the lath's direction and another at an angle varying from 30° to 50° relative to the lath's direction. Based on the literature, the auto-tempered carbides are usually known as cementite and transition-iron carbides [15,20,26,27]. However, it is reported that auto-tempered precipitation usually forms at the coarse lath of martensite [20,27]. Indeed, two types of laths developed during the martensitic transformation, driven by variations in transformation sequences and temperatures. The coarse laths developed early in the martensite formation, occurring at relatively higher temperatures and displaying a comparatively low dislocation density. This was attributed to a more extensive dislocation recovery process over an extended transformation period. In contrast, thin martensite laths formed at a later stage in the transformation, maintaining a higher dislocation density. Intra-lath carbides were associated with auto-tempered martensite. Moreover, it was observed that auto-tempered carbides tended to precipitate on the coarse martensite laths, while thin laths remained devoid of auto-tempered carbide [27]. It's worth noting that, there is not any sign of carbides in the grain boundaries in the obtained microstructure.

3.1.2. Microstructure of martensite after tempering (550 °C–30 min)

Tempering process starts with continuous heating (non-isothermal tempering) to the target temperature (550 °C). It should be noted that the changes in microstructure commence while material is subjected to continuous heating. Fig. 3 presents plots illustrating the variations in differential changes in length to temperature, depicting the transformation of martensite samples during continuous heating part of tempering for both tempering temperatures. The metallurgical phenomena, such a transition carbides precipitation, retained austenite decomposition, etc. occurring during tempering, do not produce significant length changes and identifying these slopes becomes challenging. Therefore, differential curves that show variations in expansion and contraction rates were used instead, as also reported by Ref. [28].

The changes of microstructure during the continuous heating part of tempering involve multiple stages in martensite, as reported in the literature [29]. According to the information presented in Fig. 3 (blue

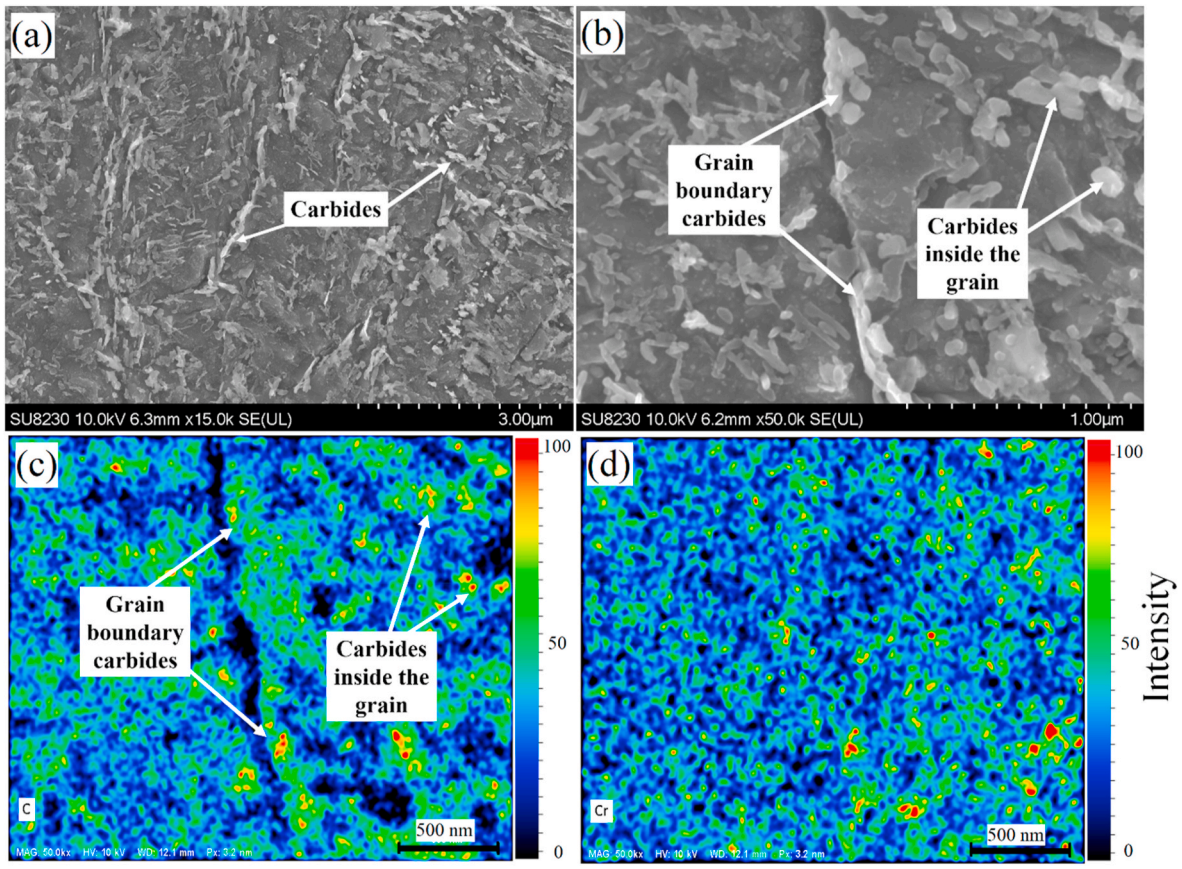

Fig. 5. SEM observation of martensite microstructure after tempering at 620 °C at lower magnification (a), higher magnification (b) and EDS mode based on carbon and chromium distributions (c) and (d), respectively.

Table 2
Composition of stable phases present during tempering at 550 °C simulated with ThermoCalc.

BCC_A2#1	Mass Fraction (%)	M23C6_D84#1	Mass Fraction (%)	M7C3_D101#1	Mass Fraction (%)	MC_ETA#1	Mass Fraction (%)
Fe	97.377	Fe	51.957	Cr	37.107	Mo	48.386
Mn	0.987	Cr	25.217	Fe	36.46	V	36.884
Ni	0.718	Mo	14.97	Mn	9.831	C	14.73
Cr	0.477	C	5.081	C	8.491	Fe	0
Si	0.353	Mn	2.394	Mo	5.986	Ni	0
Mo	0.081	Ni	0.371	V	2.076	Cr	0
V	0.005	V	0.01	Ni	0.048	Mn	0
C	0.002	Si	0	Si	0	Si	0
Volume fraction (%)	96.242	Volume fraction (%)	1.783	Volume fraction (%)	1.678	Volume fraction (%)	0.298

curve), the process involves multiple steps. The initial step, occurring below 100 °C, includes segregation and clustering, evident in a contraction observed in the dilatometry curve [30,31]. The second step involves the precipitation of transition carbides, specifically ε ($Fe_{2.4}C$) and η (Fe_2C), noted by a contraction within the temperature range of 220–280 °C [31–33]. Moving on to the third step, there is a decomposition of RA into ferrite and cementite spanning from 270 to 370 °C, accompanied by an increase in length [30,34]. The final step involves carbide precipitation, identified by a decrease in length within the temperature range of 325–375 °C [31,32]. Then the sample is maintained at the target temperature for 30 min before being cooled to room temperature.

Fig. 4 illustrates SEM image of martensite microstructure after tempering at 550 °C for 30 min. The figure depicts martensite laths; however, these laths appear blurred compared to the as-quenched microstructure. The blurring of the lath martensite following tempering is a result of substantial microstructure recovery [35].

In addition to the carbides present in the as-quenched state, tempering treatment result in precipitation at the grain boundaries and between the laths in elongated form (Fig. 4 (b)). There are two types of carbides in the microstructure, the rod-shape carbides resulting from the transformation of initial cementite inside the grain, and the elongated carbides from precipitation during tempering at the grain boundaries (Fig. 4 (b)). Fig. 4 (c) shows EDS analyses of carbon distribution in Fig. 4 (b); highlighting high carbon concentrations in the precipitations that form at the grain boundaries during tempering.

Various types of carbides with different thermal stabilities can be precipitated based on the tempering time and temperature, including, M_3C, M_2C, M_6C, M_7C_3, and $M_{23}C_6$ [14–16]. The cementite (M3C) is the first carbide to precipitate during tempering, followed by the metastable carbides. With further tempering, metastable carbides are replaced by the equilibrium carbides $M_{23}C_6$ and M_7C_3 [3,15,36]. According to Fig. 4 volume fraction of carbides inside the lath increased in comparison with auto-tempered carbides (as-quenched) in Fig. 2 due to supersaturation of the microstructure in carbon. In order to check the thermodynamic stability of the carbides, ThermoCalc was employed at 550 °C based on

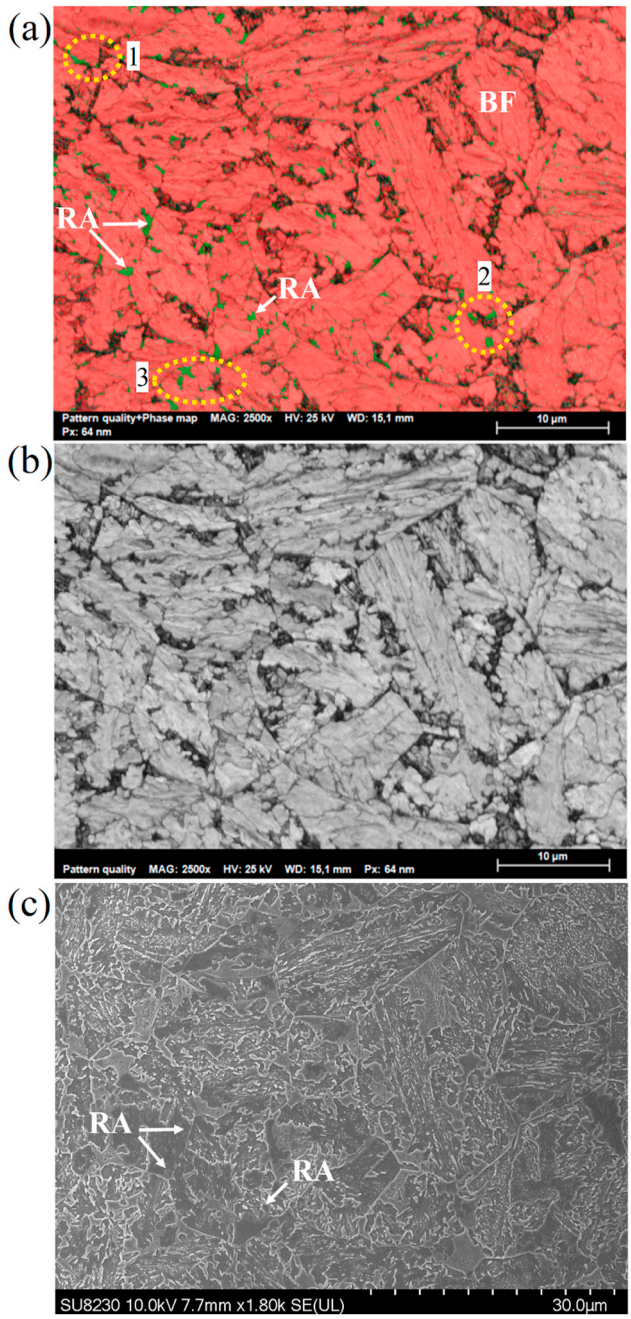

Fig. 6. EBSD phase identification map of as-quenched bainitic sample (a), quality pattern (b), and SEM observation of EBSD map zone after etching (c). Retained austenite (RA), bainitic ferrite (BF).

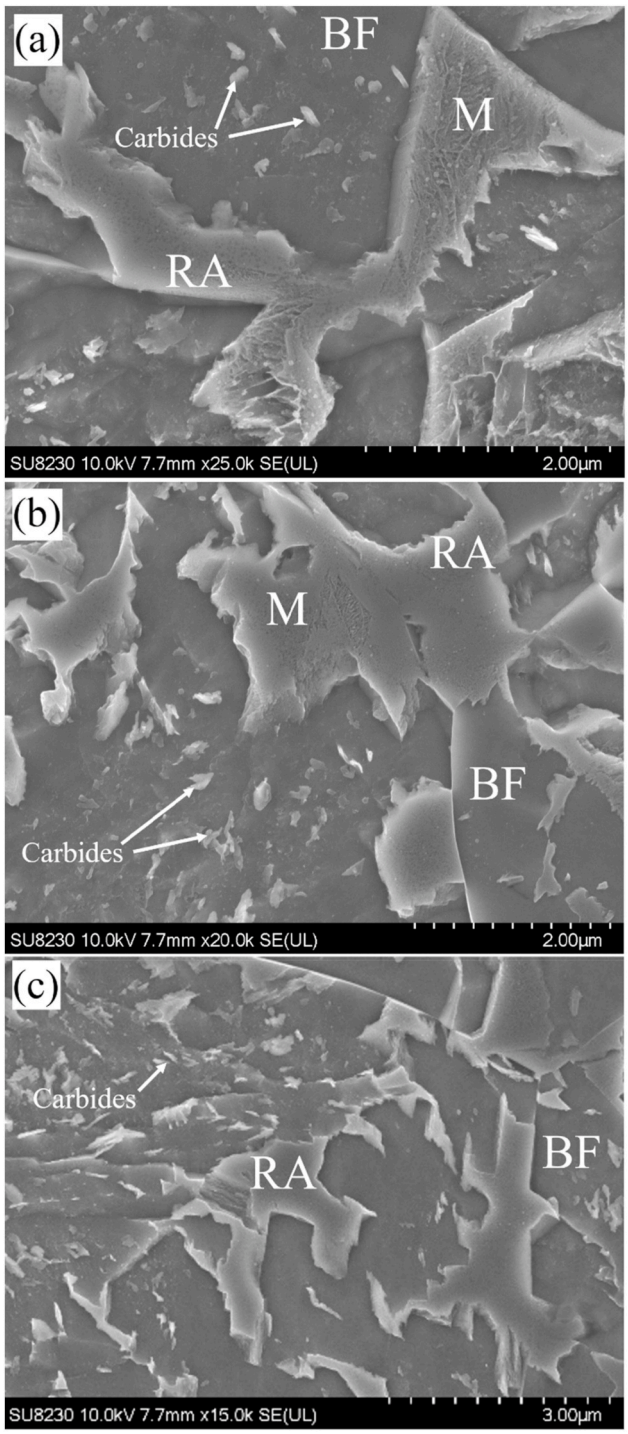

Fig. 7. SEM observation of specified zones in fig. 6 (a), zone 1 corresponds to (a), zone 2 corresponds to (b) and zone 3 corresponds to (c). Retained austenite (RA), bainitic ferrite (BF), martensite (M).

the chemical composition. ThermoCalc, as a thermodynamic software, calculates Gibbs free energies to determine phase stability, which is influenced by chemical composition and temperature. It also correlates the stable phases to their volume fraction, with more stable phases having higher volume fractions. Table 2, presents the simulated results, indicating that $M_{23}C_6$ and M_7C_3 are the stable carbides in the microstructure with volume fractions of 1.78 % and 1.67 %, respectively, while MC is the least stable carbide with a volume fraction of 0.29 %. Considering the simulated results and the featured microstructure, it can be inferred that the elongated carbides at the grain boundaries may constitute a mixture of M_7C_3 and $M_{23}C_6$. Jayan et al. [37] reported $M_{23}C_6$ as an equilibrium carbide, while M_7C_3 is metastable carbide. Nevertheless, it is probable that M_7C_3 may develop during continuous heating processes, and during holding time, the proportion of M_7C_3 could diminish while that of $M_{23}C_6$ could increase or stabilize. This explanation aligns with the expected natural carbide transformation cycle, where $M_{23}C_6$ is primarily derived from M_7C_3 [15,32].

The literature reports indicate that both carbides, particularly $M_{23}C_6$, tend to precipitate at grain boundaries, including those with a large angle, such as block and packet boundaries of martensite [15,17]. The formation of carbides at grain boundaries results from the diffusion of carbon to the boundaries of martensite laths and grains. This phenomenon is attributed to the elevated dislocation density in these regions [38].

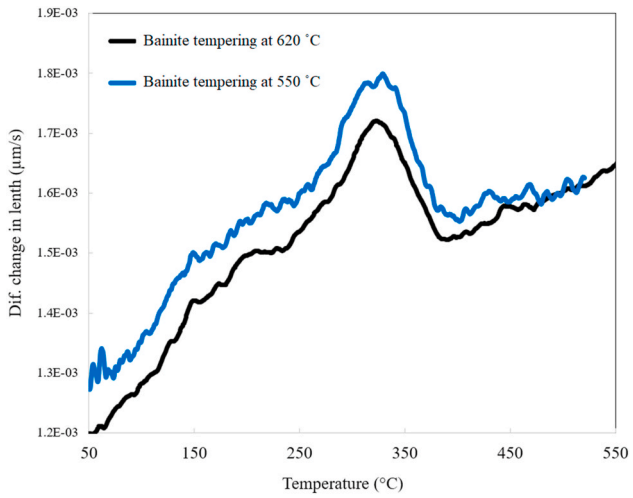

Fig. 8. Differential change in length versus temperature during continuous heating of bainite for tempering at 550 and 620 °C.

3.1.3. Microstructure of martensite after tempering (620 °C–30 min)

Fig. 5 (a) illustrates the martensite microstructure after tempering at 620 °C for 30 min. The transformations observed during continuous heating of this sample are depicted in Fig. 3 (represented by the black curve), corresponding to the phenomena elucidated in the preceding section. When compared to 550 °C, tempering at 620 °C lead to greater challenges in discerning martensite laths. The microstructure becomes more homogeneous, and the morphology of precipitates at grain boundaries changes to a more globular type. Simultaneously, there is a notable increase in the volume fraction of precipitation within the grains, taking on a more globular form (Fig. 5 (b)). Fig. 5(c) and (d) show EDS analyses of carbon and chromium distributions that confirm the carbide zones. According to the carbide formation mechanism, cementite undergoes transformation into M_7C_3, which subsequently evolves into $M_{23}C_6$ as the stable form of the carbide during tempering [15]. Coarsening of the carbides at the grain boundaries, spheroidization of the carbides inside the grains, and an increasing precipitate-free zone size are the characteristic features of tempering at 620 °C (Fig. 5(a–b)).

3.2. Tempering of bainite

3.2.1. Initial microstructure of bainite

Fig. 6(a and b) illustrates the EBSD phase map and quality pattern of bainitic microstructure after cooling at the rate of 0.05 °C/s. Fig. 6 (c) depicts SEM image of the same position in Fig. 6 (a) using the technique that was explained in the previous section. Based on the observation in Fig. 6(a) and (b), the microstructure contains bainitic sheaves represented by the red color, RA indicated in green, and areas where detection is not possible (non-indexed), visualized as dark regions.

Non-indexed or non-detectable are points in the scan for which no indexing solution could be found for the corresponding pattern. Relatively high strain misfit, and low-quality patterns are usually considered as reasons for non-indexed zones in EBSD maps [39–41]. As a result, bainitic crystals are generally more indexed in EBSD images than martensite ones, making martensite areas appear darker in contrast (somewhat poorly indexed) [42,43]. In the literature, the non-indexed areas of EBSD maps have also been considered as fresh martensitic areas, as poor crystallographic intensity indexing (compared with the bainitic areas) has been interpreted as due to the higher intensity noise caused by internal strains and dislocations [23] However, there is no proof for this claim.

In the process of bainite transformation, the matrix experiences supersaturation of carbon atoms, and these carbon atoms readily diffuse to the residual austenite, which has a high interstitial void content. This diffusion process leads to the establishment of a stable state of residual austenite. Ultimately, the M/A constituents form at locations characterized by high carbon concentrations, such as grain boundaries [44]. To investigate the non-indexed zones, three specific areas were chosen, and SEM imaging was carried out at a higher magnification for each of these regions (Fig. 7). Fig. 7 (a) corresponds to zone 1, where the green area represents a RA phase, and the black area corresponds to a non-indexed zone. As evident in the SEM image, the flat region on the left side corresponds to stable RA, indicated by the green color in the EBSD map. On the right side, the non-flat block displays clear signs of lath morphology, suggesting the possibility of residual austenite with a high carbon content that has undergone transformation to martensite. Moreover, in addition to RA and martensite, carbides are observed in the bainitic ferrite zones, as a result of precipitation during quenching. On the other hand, Fig. 7 (b), reveals the RA block undergoing partial transformation into martensite, a microstructure known as the M/A constituent. Therefore, in the EBSD map, the block displays both green area (indicating RA) and black area (representing martensite); and the same for Fig. 7 (c).

3.2.2. Microstructure of bainite after tempering (550 °C–30 min)

The tempering process for bainite, similar to martensite, initiates with continuous heating to the designated temperature. It is crucial to highlight that the changes in microstructure during the continuous heating of bainite differ from those observed in martensite [29]. Fig. 8 provides graphical representations illustrating the variations in the differential changes in length with respect to temperature. These plots depict the transformation of bainitic samples during the continuous heating phase of tempering.

In contrast to martensite, the first two steps (segregation and transition carbide precipitation) are not observed during the continuous heating step in the bainitic microstructure. This could be related to the displacive transformation of martensitic, where growth is purely restricted by the mobility of the interface [45]. In contrast, during displacive/paraequilibrium bainitic transformation, the growth of austenite ahead of the interface is governed by the diffusion of carbon [45,46]. Consequently, the paraequilibrium transformation of bainite leads to auto-tempering process which finally results in lower carbon supersaturation in bainite compared to martensite [47].

Fig. 8 reveals a distinct peak associated with the decomposition of RA in the bainitic microstructure at 325 °C. RA decomposition occurs between 270 and 370 °C for bainitic microstructures, while in martensitic microstructures, it occurs between 325 and 350 °C. In response to a difference in cooling rate, RA's volume fraction and carbon content differ [48]. Proportionally, the fraction of decomposed RA in the bainitic structure is more significant than in the martensitic one. At the end of continuous heating, the specimen is held at the target temperature for a duration of 30 min before being cooled to room temperature.

Fig. 9 shows in different magnifications the microstructure of bainite after tempering at 550 °C after 30 min. Fig. 9(a–c) indicate the decomposition of RA and M/A into an aggregated carbides zone. Large parts of M/A are transformed into chromium carbide, according to Fig. 9 (d–e), that shows higher concentrations of C and Cr in the precipitations. Aggregated carbide zones typically develop in areas with high carbon content, such as the M/A zone, as reported in the literature [44,49]. In addition, Fig. 9 (b) shows the fresh martensite zone that is formed during final cooling and confirms the incomplete decomposition of M/A zones. The fresh martensite can form from the low-carbon untransformed austenite parts [13] during the cooling to room temperature, as is confirmed indicated by dilatometry results in the following section (Fig. 13) [12].

3.2.3. Microstructure of bainite after tempering (620 °C–30 min)

The changes observed during the continuous heating phase while tempering at 620 °C resembled that explained in the previous section for 550 °C (Fig. 8). Fig. 10 illustrates microstructure of the bainite after

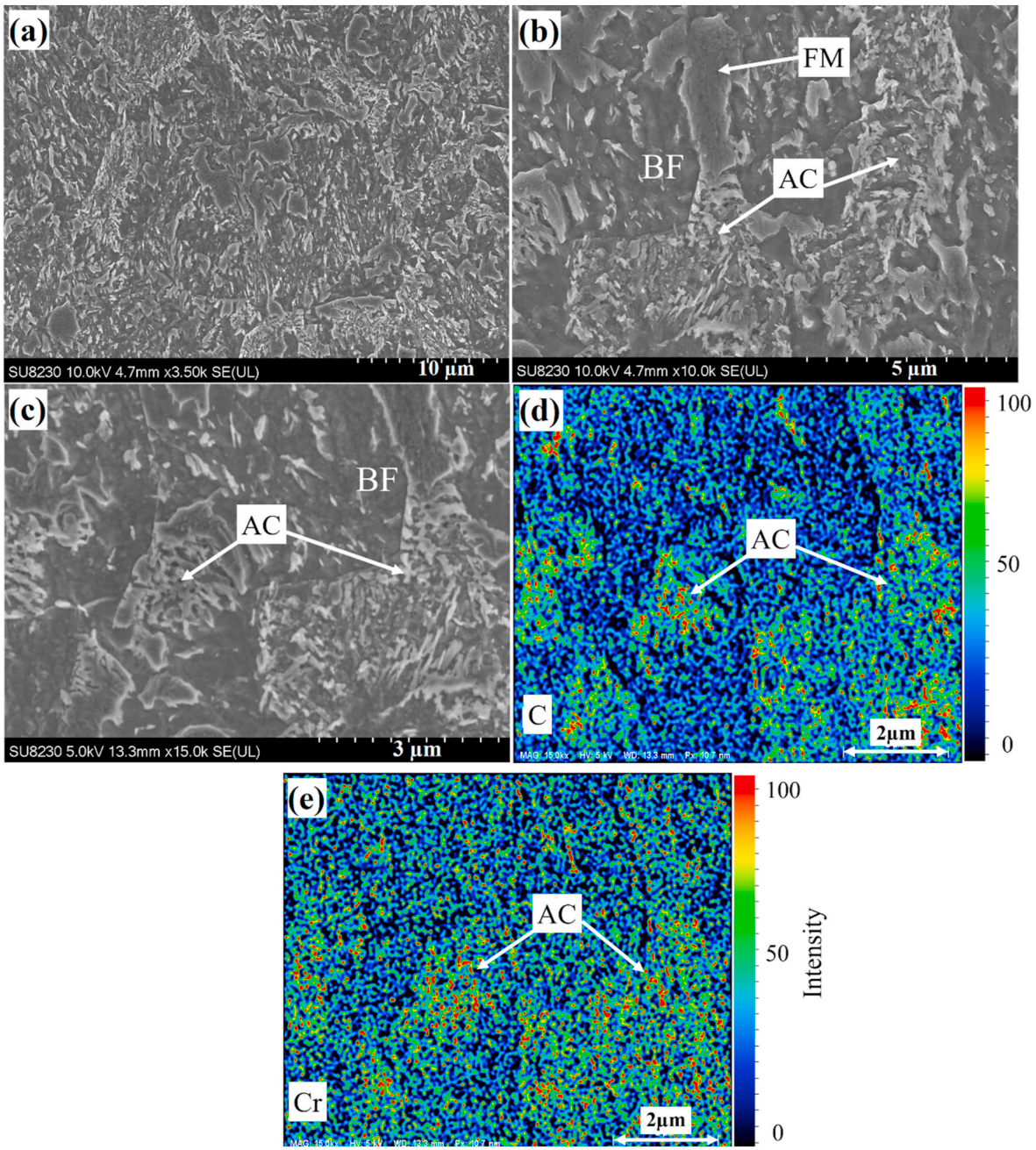

Fig. 9. SEM observation of bainitic microstructure at lower magnification after tempering at 550 °C for 30 min (a); at higher magnification (b–c); and EDS mode based on carbon and chromium distribution of image c (d and e, respectively). Fresh martensite (FM), Aggregated carbides zone (AC), bainitic ferrite (BF).

tempering at 620 °C during 30 min. It should be noted that tempering at 620 °C causes slightly different microstructure changes than the tempering at 550 °C. The primary austenite grains are still identifiable, but the morphology of the precipitation is modified. The decomposition of the M/A blocks also takes place at this temperature, but the quantity transformed is greater. Aggregated carbides form at the grain boundaries, and even inside the grains due to decomposition of M/A zones (Fig. 10(a–b)). This decomposition is still incomplete at 620 °C and the remaining parts become fresh martensite during the cooling as shown in Fig. 10 (c).

Comparing the two microstructures of Figs. 9 and 10 shows that the untransformed blocks of M/A decreased at 620 °C due to greater decomposition. On the other hand, the volume fraction of aggregated carbide zones has increased at 620 °C. For both tempering, the fresh martensitic transformation at the final cooling stage is in good agreement with the interpretations of the dilatometric cooling curves (following section, Fig. 12). Compared to the initial state, these carbides are more globular because the tempering at higher temperature increases the diffusion rate of the carbon and results in more spheroidization [13,50].

In order to analyze the bainitic microstructure in detail, an EBSD was performed on the sample tempered at 620 °C (Fig. 11 (a)). This sample underwent the preparation process for EBSD analysis before capturing the SEM image (Fig. 11 (a)). Then, as explained in section two, the Nital 5 % etchant was used for 15 s in order to highlight the microstructure (Fig. 11 (b)). Fig. 11 (a) and (b) are made at the same location to identify the zone characteristics of the microstructure. Fig. 11 (a) is pattern quality of the microstructure which shows a tempered bainite including black zones (non-indexed). Despite tempering at 620 °C, non-indexed regions are still apparent in the EBSD map. Generally, non-indexed

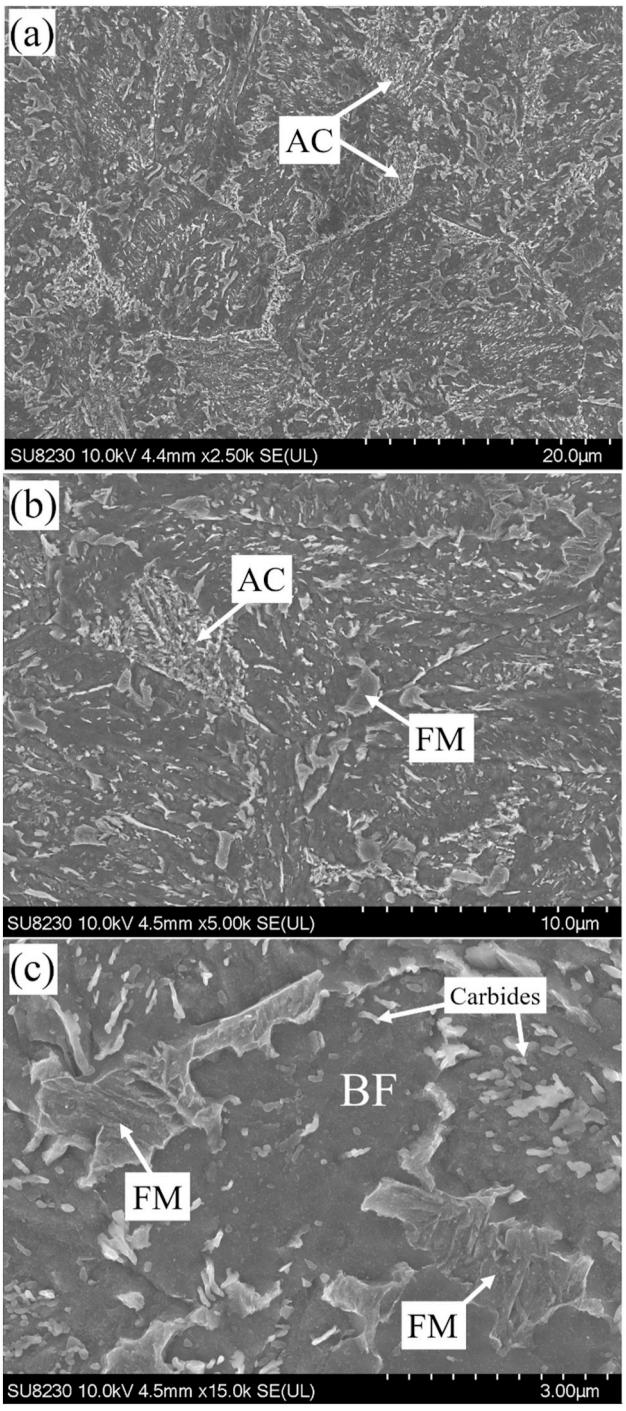

Fig. 10. SEM observation of bainitic microstructure after tempering at 620 °C at lower magnifications (a and b), and higher magnification (c). Fresh martensite (FM), Aggregated carbides zone (AC), bainitic ferrite (BF).

areas are associated with high-stress zones. However, it appears that, after tempering at a high temperature, there should be a substantial reduction in the microstructure stress [51]. In order to identify the microstructure of darker zones in Fig. 11 (a), the sample was etched and then SEM analyses were performed at the selected areas (Fig. 11(b–d)). Fig. 11(b)–(d) correspond to zones 1–3 in Fig. 11 (a), respectively.

These findings reveal that the black regions in the EBSD map consist of two distinct phases: fresh martensite and an aggregated carbide zone. In Fig. 11 (b), zone 1 is depicted as the fresh martensite microstructure which shows the stability of RA during tempering at 620 °C, and indirect decomposition during final cooling after tempering. Fig. 11 (c) and (d) represent zones 2 and 3 respectively, which display casing aggregated carbide zones. EDS analysis, focusing on C and Cr distributions, indicates the aggregated of chromium carbides, as depicted in Fig. 11(e–f). In this study, an observation aligning with existing literature indicates that high-stress regions, such as martensite, are typically recognized as non-indexed areas in EBSD analysis. In completing the previous information in the literature, the current research demonstrates that areas with a high density of carbides are also manifested as non-indexed regions in the EBSD.

Fig. 12 illustrates the change in length as a function of temperature at the final stage of cooling for the bainitic sample. It should be mentioned that the cooling curves in the martensite samples exhibit a consistent slope. Fig. 12 shows that at the final stage of cooling to room temperature after tempering, some signs of expansion are observed at 140 and 240 °C for tempering at 550 and 620 °C, respectively. The expansion during the final cooling after tempering could be related to the indirect decomposition of blocky M/A or RA to fresh martensite. It's important to highlight that, as a result of the decomposition occurring in the isothermal tempering procedure, the formation of carbides causes a reduction in the carbon content within RA, consequently reducing its stability. Thus, during the subsequent cooling phase, a transition to fresh martensite occurs. The difference in decomposition at cooling is related to the carbon content of the M/A or RA. It is supposed that tempering at 620 °C leads to higher carbides fraction formation, which results in lower carbon content of the RA and M/A. Therefore, transformation to the fresh martensite happens at higher temperature in comparison with tempering at 550 °C.

The stability of RA during tempering at 620 °C was evaluated using the DICTRA module of the ThermoCalc software. However, to conduct the simulation, the carbon content of the RA resulting from the whole tempering process must be included as input. The following approach was used for this determination: Initially, different empirical equations that provide Ms as a function of the chemical composition were examined. The equation reported by Tamura [52]:

$$Ms = 550 - 361X_c - 39X_{Mn} - 20X_{Cr} - 5X_{Mo} - 34X_{Ni} - 30X_{Al} + 15X_{Co} - 10X_{Cu} - 35X_V$$

Equation 1

provided the closest Ms value to that of the investigated steel, which was determined by dilatometry (350 °C) and presented in Ref. [53]. Next, using the Ms temperature of FM at 620 °C, which is 240 °C (Fig. 12), and the above equation, the carbon content of the RA at the end of the tempering cycle was estimated to be 0.56 wt%. Finally, using the chemical composition of the RA, the DICTRA simulation was conducted and the results are reported in Fig. 13. The results reveal that approximately 53 % of the RA decomposes during the first 30 min, while the remaining portion remains nearly stable and transforms to FM during final cooling. The above findings further confirm those from microstructure analysis, reported in Fig. 10 and dilatometry results presented in Fig. 12 thereby providing an additional confirmation of the incomplete decomposition of RA at 620 °C in the investigated steel.

3.3. Differences between tempered microstructures

Fig. 14 (a) depicts a schematic illustrating the evolution of the as-quenched microstructure during tempering. This diagram is based on previous analyses and information from the literature review. Before tempering, the martensite is lathed with the M_3C auto-tempered carbides inside the lathes. Then with the tempering at 550 °C an elongated $M_{23}C_6$ and M_7C_3 precipitation forms at the grain boundaries, accompanied by a spheroidization of M_3C within the lathes. The increase in the tempering temperature to 620 °C leads to the aggregation and spheroidization of all the carbides. In addition, the tempering leads to a widening of the laths. It's important to note that there are no discernible

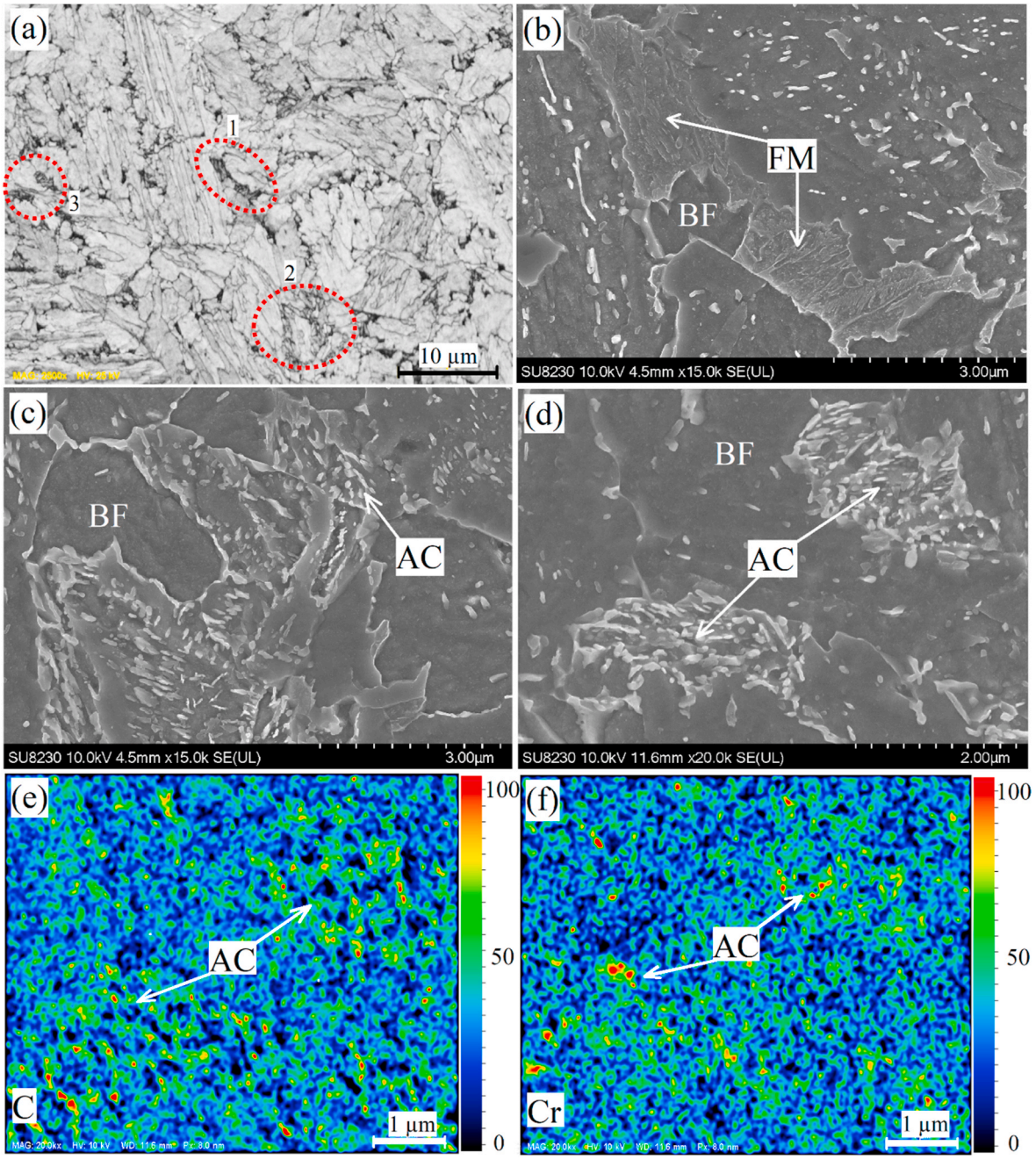

Fig. 11. Quality pattern of bainitic microstructure after 30 min tempering at 620 °C (a), SEM observation of figures after etching of different selected zone in (a), zones 1 (b), zone 2 (c), zone 3 (d); and EDS analyses of zone 3 based on carbon and chromium distributions (e and f, respectively).

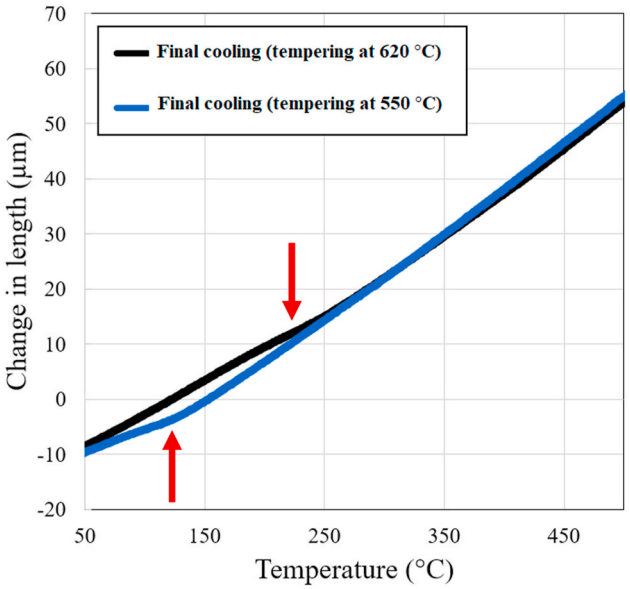

Fig. 12. Dilatometric curve (change in length as a function of temperature) during cooling of bainite at the rate of 1 °C/s after tempering at 550 °C and 620 °C.

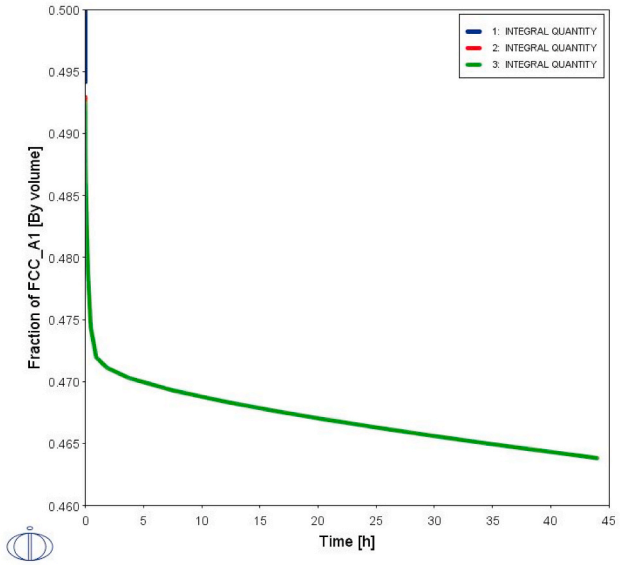

Fig. 13. Evolution of the retained austenite (RA) volume fraction during tempering at 620 °C as function of the time simulated by DICTRA.

signs of aggregated carbide zones in the martensitic sample after tempering, primarily due to the absence of M/A zones.

Fig. 14 (b) summarizes the evolution of M/A blocks in the bainitic microstructure during tempering. Before tempering, the bainite contains RA and M/A blocks at the grain boundaries and auto-tempered carbides. The tempering makes it possible for these two secondary phases to decompose into carbides. When the decomposition of M/A is incomplete, there is a transformation of the remainder into fresh martensite at the final cooling stage. Increasing the temperature causes a more advanced decomposition, leading to a lower percentage of fresh martensite and higher carbides at the end of the heat treatment. In addition, the decomposition of M/A in the final stages leads to the formation of a chain of aggregated carbide zones at the grain boundaries.

Fig. 15 illustrates the hardness of the samples after processing as a function of the tempering temperature. The hardness after quenching shows 505 ± 6 and 370 ± 17 HV for martensite and bainite, respectively. As a result of displacive transformation, martensite is at its maximum hardness before tempering, because it contains a high percentage of supersaturated carbon and is characterized by lattice shear deformation [21,54]. By contrast, 26 % lower in hardness of the bainitic sample can be related to the higher fraction of RA [55,56].

The hardness of martensite after tempering at 550 °C and 620 °C, decreases to 413 ± 10 and 381 ± 8 HV, respectively. The softening mechanism of martensite can be explained by several phenomena such as; decreasing dislocation density [27], reduction of tetragonality of the martensite [57], and spheroidization of the carbides [58]. The overall hardness of a steel obviously depends on the precipitates obtained during treatment, but the main factor affecting this hardness is the matrix. According to the literature [59,60], the hardness of M_7C_3 is between 1050 and 1500 HV while $M_{23}C_6$ seems to have a lower hardness between 900 and 1400 HV. This aspect can accentuate the difference between the two tempering temperatures. On the one hand, at 550 °C, $M_{23}C_6$ precipitation increases at the expense of M_7C_3 carbide with, in parallel, the diffusion of carbon leading to a reduction in hardness. On the other hand, at 620 °C, the transformation between the carbides continues and the spheroidization is more active, which decreases the hardness significantly. However, Fig. 5(c–d) confirms the coarsening and spheroidization of the carbides and the decreasing carbon content of the matrix as a main cause of the drop in hardness. There is no sign of secondary hardening during tempering of the martensite in Fig. 15. It seems that during tempering at 550 and 620 °C, chromium carbides are already precipitated. However, further tempering tests at lower temperatures would be required to observe this phenomena [61].

Before tempering, the bainite exhibit an average hardness of 370 ± 10 HV. Initially, tempering at 550 °C increases the hardness to 390 ± 10 HV, and then decreases to 373 ± 5 HV after tempering at 620 °C. The increasing hardness after tempering of bainitic microstructure has already been reported [22,62,63]. According to the literature, the increase in hardness after tempering is attributed to the secondary hardening process [63]. However, according to the results of this study as shown in Fig. 10 (c) and Fig. 11 (c and e), transformation of RA to fresh martensite at the final cooling stages also should be considered as an important factor. The process of decomposition of RA at the final cooling stage of tempering is known as an indirect decomposition of RA, and is reported by several researchers [10,64,65]. Finally, the higher hardness observed after tempering at 550 °C compared to 620 °C may be attributed to a greater volume fraction of fresh martensite formed.

4. Conclusions

The influence of the as-quenched microstructure and tempering temperature on the ultimate microstructure and hardness was examined in medium-carbon, low-alloy steel. The present investigation yields the following conclusions.

- Auto-tempered carbides were identified within the as-quenched microstructure, including both bainite and martensite phases.
- While tempering the martensite microstructure at 550 °C, there is an augmentation in the volume fraction of carbides within the laths, accompanied by the precipitation of elongated carbides along the lath and grain boundaries, increasing the tempering temperature to 620 °C induces the spheroidization of both inter- and intra-lath carbides.
- Tempering granular bainite at 550 and 620 °C is accompanied by an incomplete decomposition of RA and the formation of fresh martensite during the final cooling stages. Decomposition of M/A zones to aggregated chromium carbides zones is observed after tempering at the grain boundaries.
- An increase in hardness was observed in the bainitic sample; however, no such increase was noted in the martensitic sample. This

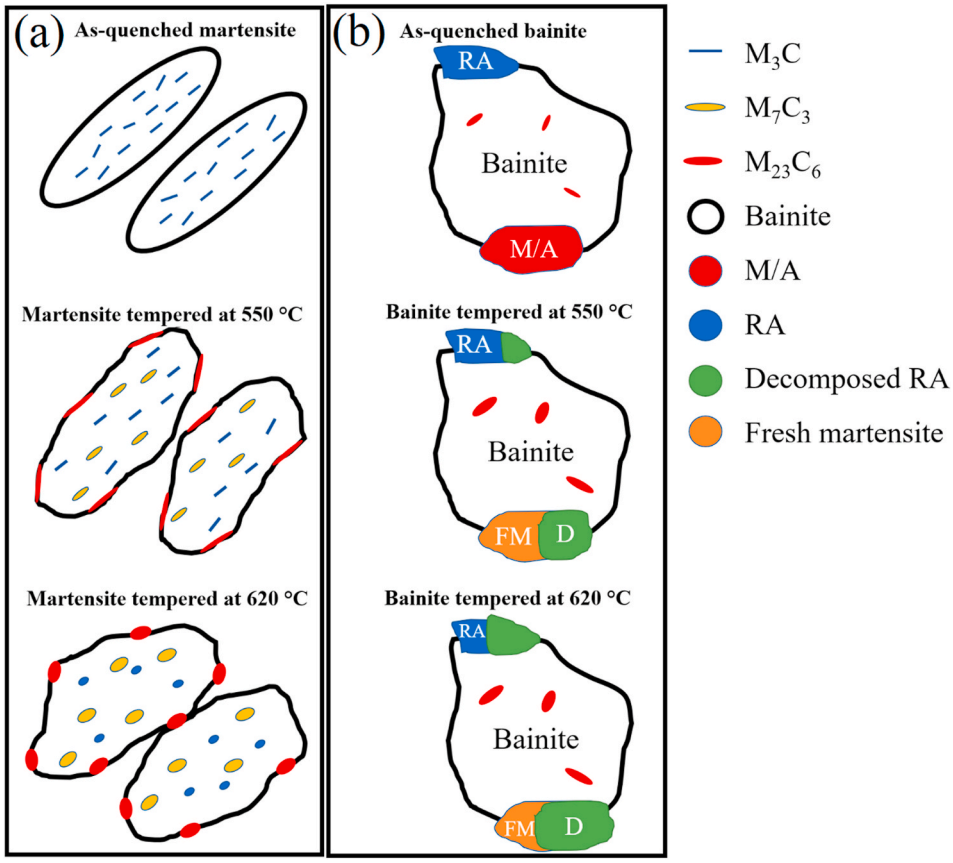

Fig. 14. Schematic representation of the microstructure evolution of as-quenched martensite and bainite after tempering at 550 and 620 °C for 30 min.

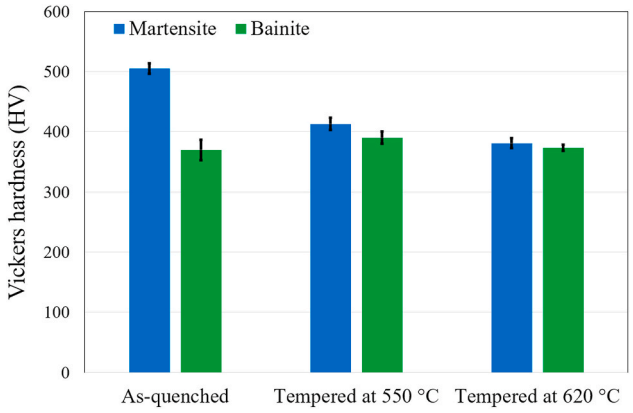

Fig. 15. Evolution of martensite and bainite hardness after tempering at 550 °C and 620 °C for 30 min, with heating at 0.2 °C/s and cooling at 1 °C/s.

discrepancy can be attributed to the formation of fresh martensite resulting from the incomplete decomposition of RA.

CRediT authorship contribution statement

Ehsan Tolouei: Writing – original draft. **Valentin Hurel:** Writing – review & editing, Data curation. **Abdelhalim Loucif:** Writing – review & editing. **Jean-Benoit Morin:** Writing – review & editing, Validation. **Mohammad Jahazi:** Supervision, Project administration.

Declaration of competing interest

The authors declare that they have no known competing financial interests or personal relationships that could have appeared to influence the work reported in this paper.

Data availability

The data that has been used is confidential.

References

[1] D. Firrao, et al., A C C I A I O Heat treatment and failure risk of large automotive plastic molds: a fracture mechanics approach and property assessment, Metallurgia Italiana 98 (2006).
[2] Y.F. Zheng, et al., Continuous cooling transformation behaviour and bainite formation kinetics of new bainitic steel, Mater. Sci. Technol. 33 (4) (2017) 454–463.
[3] S.H. Talebi, M. Jahazi, H. Melkonyan, Retained austenite decomposition and carbide precipitation during isothermal tempering of a medium-carbon low-alloy bainitic steel, Materials 11 (8) (2018) 1441.
[4] A. Loucif, et al., Evolution of A-type macrosegregation in large size steel ingot after multistep forging and heat treatment, Metall. Mater. Trans. B 49 (3) (2018) 1046–1055.
[5] S.H. Talebi, et al., In situ study of phase transformations during non-isothermal tempering of bainitic and martensitic microstructures, Metals 7 (9) (2017).
[6] Y. Bouissa, et al., Microstructure-based FEM modeling of phase transformation during quenching of large-size steel forgings, Metall. Mater. Trans. 52 (5) (2021) 1883–1900.
[7] S.M. Chentouf, et al., Characteristics of austenite transformation during post forge cooling of large-size high strength steel ingots, Metallography, Microstructure, and Analysis 3 (4) (2014) 281–297.
[8] A.S. Podder, Tempering of a mixture of bainite and retained austenite, in: Department of Materials Science and Metallurgy, University of, Cambridge, 2011.
[9] G. Yan, et al., Characteristic of retained austenite decomposition during tempering and its effect on impact toughness in SA508 Gr.3 steel, J. Nucl. Mater. 483 (2017) 167–175.

[10] C. Lerchbacher, S. Zinner, H. Leitner, Direct or indirect: influence of type of retained austenite decomposition during tempering on the toughness of a hot-work tool steel, Materials Science and Engineering: A 564 (2013) 163–168.
[11] Z. Jiang, et al., The tempering behavior of martensite/austenite islands on the mechanical properties of a low alloy Mn-Ni-Mo steel with granular bainite, Mater. Today Commun. 26 (2021) 102166.
[12] V. Ruiz-Jimenez, et al., Retained austenite destabilization during tempering of low-temperature bainite, Appl. Sci. 10 (24) (2020) 8901.
[13] W. Zhao, et al., Study on diversified carbide precipitation in high-strength low-alloy steel during tempering, Steel Res. Int. 92 (7) (2021) 2000723.
[14] D.R.G. Mitchell, C.J. Ball, A quantitative X-ray diffraction and analytical electron microscopy study of service-exposed 2.25Cr–1Mo steels, Mater. Char. 47 (1) (2001) 17–26.
[15] S. Dépinoy, et al., Carbide precipitation in 2.25 Cr-1 Mo bainitic steel: effect of heating and isothermal tempering conditions, Metall. Mater. Trans. 48 (5) (2017) 2164–2178.
[16] T.P. Hou, Y. Li, K.M. Wu, Effect of high magnetic field on alloy carbide precipitation in an Fe–C–Mo alloy, J. Alloys Compd. 527 (2012) 240–246.
[17] M. Taneike, K. Sawada, F. Abe, Effect of carbon concentration on precipitation behavior of M23C6 carbides and MX carbonitrides in martensitic 9Cr steel during heat treatment, Metall. Mater. Trans. 35 (4) (2004) 1255–1262.
[18] A.T.W. Barrow, J.H. Kang, P.E.J. Rivera-Díaz-del-Castillo, The $\epsilon \rightarrow \eta \rightarrow \theta$ transition in 100Cr6 and its effect on mechanical properties, Acta Mater. 60 (6) (2012) 2805–2815.
[19] S. Mayer, et al., Changes in tempering and its effect on precipitation behaviour in a hot-work tool steel, Steel Res. Int. 80 (1) (2009) 89–95.
[20] D. Ning, et al., Carbide precipitation and coarsening kinetics in low carbon and low alloy steel during quenching and subsequently tempering, Mater. Char. 176 (2021) 111111.
[21] G. Krauss, 5 - tempering of martensite in carbon steels, in: E. Pereloma, D. V. Edmonds (Eds.), Phase Transformations in Steels, Woodhead Publishing, 2012, pp. 126–150.
[22] Y. Luo, et al., Effect of tempering on microstructure and mechanical properties of a non-quenched bainitic steel, Materials Science and Engineering: A 527 (15) (2010) 3433–3437.
[23] D. De Knijf, et al., Effect of fresh martensite on the stability of retained austenite in quenching and partitioning steel, Materials Science and Engineering: A 615 (2014) 107–115.
[24] Thermodynamic Databases. Available from: https://thermocalc.com/products/databases/.
[25] C.E.I.C. Ohlund, E. Schlangen, S. Erik Offerman, The kinetics of softening and microstructure evolution of martensite in Fe–C–Mn steel during tempering at 300°C, Materials Science and Engineering: A 560 (2013) 351–357.
[26] Talebi, S.H., Microstructure evolution and optimization of the tempering heat treatment of a medium-carbon low-alloy steel, in Mechanic. 2018, ÉCOLE DE TECHNOLOGIE SUPÉRIEURE. p. 123.
[27] D.C. Saha, et al., Effects of tempering mode on the structural changes of martensite, Materials Science and Engineering: A 673 (2016) 467–475.
[28] B. Pawłowski, P. Bała, R. Dziurka, Improper interpretation of dilatometric data for cooling transformation in steels, Arch. Metall. Mater. 59 (2014) 1159–1161.
[29] H. Talebi, et al., Influence of starting microstructure on dilatation behavior during tempering of a high strength steel, Mater. Sci. Forum 941 (2018) 305–310.
[30] S.H. Talebi, et al., In situ study of phase transformations during non-isothermal tempering of bainitic and martensitic microstructures, Metals 7 (9) (2017) 346.
[31] P.V. Morra, A.J. Böttger, E.J. Mittemeijer, Decomposition of Iron-based Martensite. A kinetic analysis by means of differential scanning calorimetry and dilatometry, Journal of Thermal Analysis and Calorimetry 64 (3) (2001) 905–914.
[32] S.H. Talebi, M. Jahazi, H. Melkonyan, Retained austenite decomposition and carbide precipitation during isothermal tempering of a medium-carbon low-alloy bainitic steel, Materials 11 (8) (2018) 1441.
[33] F.G. Caballero, M.K. Miller, C. Garcia-Mateo, Influence of transformation temperature on carbide precipitation sequence during lower bainite formation, Mater. Chem. Phys. 146 (1) (2014) 50–57.
[34] L. Cheng, et al., The tempering of iron- carbon martensite; dilatometric and calorimetric analysis, Metall. Trans. A 19 (10) (1988) 2415–2426.
[35] Y.-j. Zhao, et al., Effect of tempering on microstructure and mechanical properties of 3Mn-Si-Ni martensitic steel, Materials Science and Engineering: A 711 (2018) 397–404.
[36] J.B. Lee, et al., Kinetics of carbide formation for quenching and tempering steels during high-frequency induction heat treatment, Mater. Chem. Phys. 129 (1) (2011) 365–370.
[37] V. Jayan, M.Y. Khan, M. Hussain, X-ray investigation of solid solution partitioning in 2.25Cr-1Mo steel after extended elevated temperature service in power station, Mater. Sci. Technol. 19 (11) (2003) 1546–1552.
[38] A. Vieweg, et al., Phase evolution and carbon redistribution during continuous tempering of martensite studied with high resolution techniques, Mater. Des. 136 (2017) 214–222.
[39] B.-Y. Jeong, R. Gauvin, S. Yue, EBSD study of martensite in a dual phase steel, Microsc. Microanal. 8 (S02) (2002) 700–701.
[40] N. Isasti, et al., Analysis of complex steel microstructures by high-resolution EBSD, JOM 68 (1) (2016) 215–223.
[41] M.-S. Baek, et al., Quantitative phase analysis of martensite-bainite steel using EBSD and its microstructure, tensile and high-cycle fatigue behaviors, Materials Science and Engineering: A 785 (2020) 139375.
[42] S. Pashangeh, et al., Detection and estimation of retained austenite in a high strength Si-bearing bainite-martensite-retained austenite micro-composite steel after quenching and bainitic holding (Q& B), Metals 9 (5) (2019) 492.
[43] A. Navarro-López, et al., Characterization of bainitic/martensitic structures formed in isothermal treatments below the Ms temperature, Mater. Char. 128 (2017) 248–256.
[44] B. Wang, et al., Sensitivity of the impact toughness and microstructure of 15CrNi3MoV steel under different quenching rates, Acta Metall. Sin. 36 (10) (2023) 1735–1748.
[45] G.B. Olson, H.K.D.H. Bhadeshia, M. Cohen, Coupled diffusional/displacive transformations, Acta Metall. 37 (2) (1989) 381–390.
[46] M. Santofimia, et al., Evaluation of displacive models for bainite transformation kinetics in steels, Mater. Trans. 47 (6) (2006) 1492–1500.
[47] H. Bhadeshia, Bainite in Steels: Transformation, Microstructure and Properties, The Institute of Materials, University of Cambridge, London, 2001, pp. 377–382.
[48] F.C. An, et al., Incompleteness of bainite transformation in quenched and tempered steel under continuous cooling conditions, J. Mater. Res. Technol. 9 (4) (2020) 8985–8996.
[49] C.W. Li, et al., Effect of tempering temperature on the microstructure and mechanical properties of a reactor pressure vessel steel, J. Nucl. Mater. 477 (2016) 246–256.
[50] P. Thibaux, A. Métenier, C. Xhoffer, Carbon diffusion measurement in austenite in the temperature range 500 °C to 900 °C, Metall. Mater. Trans. 38 (6) (2007) 1169–1176.
[51] O. Haiko, et al., The effect of tempering on the microstructure and mechanical properties of a novel 0.4C press-hardening steel, Appl. Sci. 9 (20) (2019) 4231.
[52] T. I, Steel Material Study on the Strength, Nikkan Kogyo Shinbun Ltd, Tokyo, 1970, p. 40.
[53] Hurel, V., Optimazation of the heat treatment of a steel with high mechanical resistance, in Mechanic. 2022, Ecole de technology superior.
[54] Bhadeshia, H. and R. Honeycombe, Steels - Microstructure and Properties (fourth ed.). Elsevier.
[55] B. Adamczyk-Cieślak, et al., The impact of retained austenite on the mechanical properties of bainitic and dual phase steels, J. Mater. Eng. Perform. 31 (6) (2022) 4419–4433.
[56] F. Hu, et al., Refinement of retained austenite in super-bainitic steel by a deep cryogenic treatment, ISIJ Int. 54 (1) (2014) 222–226.
[57] I. Tkalcec, et al., Tempering effects on a martensitic high carbon steel, Materials Science and Engineering: A 387–389 (2004) 352–356.
[58] Bhadeshia, H. and R. Honeycombe, Steels - Microstructure and Properties (fourth ed.). Elsevier. p. 244.
[59] H. Berns, Hartlegierungen und Hartverbundwerkstoffe: Gefüge, Eigenschaften, Bearbeitung, Anwendung, Springer Berlin Heidelberg, 1998.
[60] S. Buytoz, Microstructural properties of M7C3 eutectic carbides in a Fe–Cr–C alloy, Mater. Lett. 60 (5) (2006) 605–608.
[61] Bhadeshia, H. and R. Honeycombe, Steels - Microstructure and Properties (fourth ed.). Elsevier. p. 259.
[62] B.M. Huang, et al., Secondary hardened bainite, Mater. Sci. Technol. 30 (9) (2014) 1014–1023.
[63] J. Kang, et al., Effect of tempering on the microstructure and mechanical properties of a medium carbon bainitic steel, Materials Science and Engineering: A 686 (2017) 150–159.
[64] M. Slingerland, L. Borghouts, Direct and indirect influence of physical education-based interventions on physical activity: a review, J Phys Act Health 8 (6) (2011) 866–878.
[65] A. Saha Podder, H.K.D.H. Bhadeshia, Thermal stability of austenite retained in bainitic steels, Materials Science and Engineering: A 527 (7) (2010) 2121–2128.